Coatomer and dimeric ADP ribosylation factor 1 promote distinct steps in membrane scission

Rainer Beck,[1] Simone Prinz,[2] Petra Diestelkötter-Bachert,[1] Simone Röhling,[1] Frank Adolf,[1] Kathrin Hoehner,[1] Sonja Welsch,[2] Paolo Ronchi,[3] Britta Brügger,[1] John A.G. Briggs,[2,3] and Felix Wieland[1]

[1]Heidelberg University Biochemistry Center, Heidelberg University, 69120 Heidelberg, Germany
[2]Structural and Computational Biology Unit and [3]Cell Biology and Biophysics Unit, European Molecular Biology Laboratory, 69117 Heidelberg, Germany

Formation of coated vesicles requires two striking manipulations of the lipid bilayer. First, membrane curvature is induced to drive bud formation. Second, a scission reaction at the bud neck releases the vesicle. Using a reconstituted system for COPI vesicle formation from purified components, we find that a dimerization-deficient Arf1 mutant, which does not display the ability to modulate membrane curvature in vitro or to drive formation of coated vesicles, is able to recruit coatomer to allow formation of COPI-coated buds but does not support scission. Chemical cross-linking of this Arf1 mutant restores vesicle release. These experiments show that initial curvature of the bud is defined primarily by coatomer, whereas the membrane curvature modulating activity of dimeric Arf1 is required for membrane scission.

Introduction

Coated vesicle formation generally requires GTPases and coat protein complexes. In the secretory pathway, small GTPases are used to initiate coat recruitment: Sar1p for COPII-coated vesicles and Arf1 for COPI- and clathrin-coated vesicles. Next, the membrane is sculpted to form a bud, and finally, membrane separation takes place to complete vesicle formation. In endocytosis, the scission of clathrin-coated vesicles containing AP2 is performed by the GTPase dynamin (Pucadyil and Schmid, 2009). The mechanism of the final stage leading to membrane separation in the COPI and COPII systems, however, is less clear. In contrast to the action of dynamin, which requires the consumption of GTP, scission of COPII and COPI vesicles can take place when GTP hydrolysis is blocked, as indicated from various reconstitution systems using biological membranes as well as liposomes (Malhotra et al., 1989; Serafini and Rothman, 1992; Barlowe et al., 1994; Matsuoka et al., 1998; Spang et al., 1998; Bremser et al., 1999). Studies in the COPII system have suggested that the small GTPase Sar1 directly initiates membrane curvature during COPII vesicle biogenesis and takes part in vesicle scission from the ER (Barlowe et al., 1994; Lee et al., 2005). A further study indicated that Sar1p-mediated membrane scission depends on formation of a scaffold of the small GTPase on the membrane, independent of the other COPII coat components (Long et al., 2010).

In the COPI system, free vesicles can be generated in vitro from isolated Golgi membrane fractions (Spang et al., 1998; Bremser et al., 1999) or in chemically defined liposomal systems, with Arf1 and coatomer as the minimal components required (Malhotra et al., 1989; Sönnichsen et al., 1996; Malsam et al., 2005; Weimer et al., 2008; Beck et al., 2009a; Rutz et al., 2009). Although a role for additional protein factors in COPI vesicle scission has been suggested (Yang et al., 2005), such factors are not required in chemically defined reconstitution systems. Thus, in the most basic mechanism for COPI vesicle generation, Arf1-GTP and coatomer should act in concert to sculpt the membrane to form a bud and, subsequently, bring about membrane separation.

Here, we investigate the molecular mechanisms that underlie the formation of curvature and subsequent scission of a coated vesicle. Previously, we and others have reported that Arf1 has the ability to modulate the shape of liposomal bilayers (henceforth called membrane surface activity; Beck et al., 2008; Krauss et al., 2008; Lundmark et al., 2008). We now show that it is coatomer that sculpts the curvature of a membrane bud and

Correspondence to Felix Wieland: felix.wieland@bzh.uni-heidelberg.de; or John A.G. Briggs: briggs@embl.de

Abbreviations used in this paper: Arf, ADP ribosylation factor; ArfGAP, Arf GTPase-activating protein; ARNO, Arf nucleotide binding site opener; BMH, bismaleimidohexane; Bp, *p*-benzoyl-L-phenylalanine; GalT, galactosyltransferase; GUV, giant unilamellar vesicle; mol%, mole percent; $PI(4,5)P_2$, phosphatidylinositol-4,5-bisphosphate; wt, wild type.

The Rockefeller University Press $30.00
J. Cell Biol. Vol. 194 No. 5 765–777
www.jcb.org/cgi/doi/10.1083/jcb.201011027

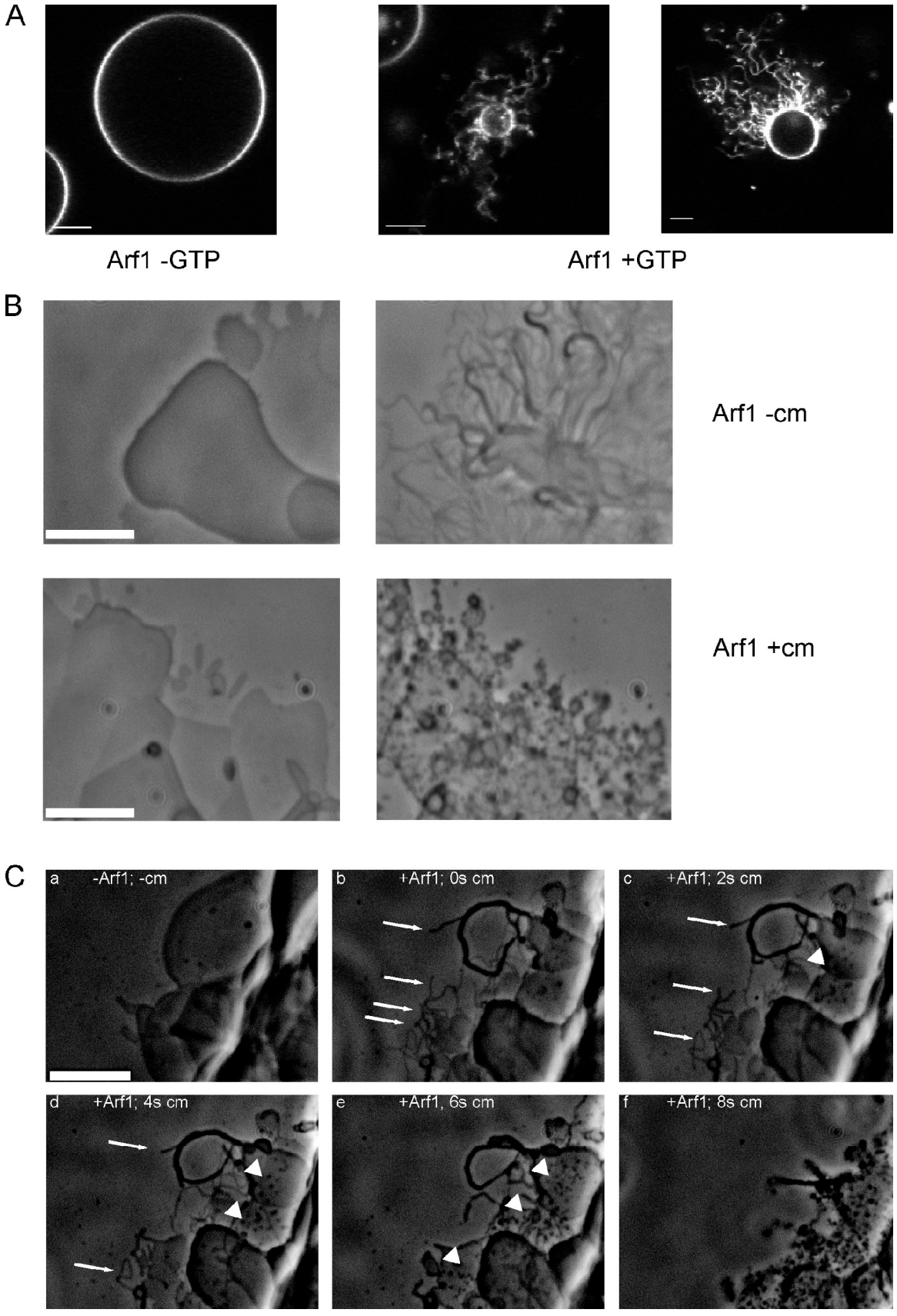

Figure 1. **Membrane surface activity of Arf1 and coatomer.** (A) Membrane surface activity of Arf1 analyzed in GUVs. GUVs containing 0.5 mol% 1,2-dipalmitoyl-*sn*-glycero-3-phosphoethanolamine-*N*-lissamine rhodamine B sulfonyl were incubated with 3.5 µM Arf1-wt and 0.4 µM ARNO in the presence or absence of 1 mM GTP as indicated and recorded in a confocal laser-scanning microscope (LSM 510; Carl Zeiss) with a 63× objective lens and a pinhole

that the membrane surface activity of Arf1 is not involved in bud formation but rather is required for scission. We further present a novel mechanistic model in which dimerization of a small GTPase plays a key role in vesicle scission.

Results

Arf1 is required for scission of COPI vesicles

Recently, Arf1 was shown to induce positive curvature on membranes (Beck et al., 2008; Krauss et al., 2008; Lundmark et al., 2008) by either monitoring tubulation of membrane sheets in light microscopy or EM of tubulated liposomes. Although we showed that this tubulation activity of Arf1 is ultimately required for vesicle biogenesis (Beck et al., 2008), it is unknown whether this activity is actually bending the membrane physically during COPI vesicle formation. Thus, we henceforth use the term "membrane surface activity" when we refer to Arf1-induced changes on liposomal bilayer morphology. This allows discriminating membrane surface activity of Arf1 and membrane curvature, which is ultimately induced on the Golgi membrane to form a vesicle bud during vesicle biogenesis.

As an alternative approach to the published data mentioned in the first paragraph, we monitored Arf1-GTP–induced membrane surface activity on giant unilamellar vesicles (GUVs) by confocal microscopy using either C-terminally fluorescently labeled Arf1, fluorescently labeled GTP (not depicted), or fluorescently labeled phospholipids (Fig. 1 A). GTP-dependent tubulation of GUVs occurred at Arf1 concentrations of 2–5 µM. When Arf1 concentrations of 0.5 µM and below were used, membrane deformation was not observed, in agreement with previous observations (Manneville et al., 2008).

As a next step, we asked whether the presence of a coatomer would have a contribution to Arf1-mediated membrane surface activity by analyzing membrane sheets in a phase-contrast light microscopy assay (Roux et al., 2006; Beck et al., 2008; Krauss et al., 2008). After addition of Arf1, the guanine nucleotide exchange factor ADP ribosylation factor (Arf) nucleotide binding site opener (ARNO; Chardin et al., 1996), and GTP to a hydrated lipid surface in the absence of coatomer, planar lipid sheets (Fig. 1 B, left) were converted into tubules (Fig. 1 B, top right; in line with Beck et al., 2008). This effect presumably results from the insertion of Arf1's amphipathic helix into the membrane (Antonny et al., 1997), possibly with its myristoyl residue perpendicular to the membrane lipid acyl chains (Liu et al., 2010). In experiments to control for a contribution to this membrane surface activity of Arf's N-terminal myristoylated amphipathic helix, we used a His-tagged truncated protein lacking the amphipathic helix, NΔ17-Arf1, on membrane sheets containing 5 mol percent (mol%) Ni^{++} lipids. This allows the truncated protein to be recruited via His_6–Ni^{++} interaction (Fig. S1). Arf1 lacking its N-terminal amphipathic helix exerted no membrane surface activity (Video 1). This is in line with a study on a similar function for Sar1p (Lee et al., 2005), demonstrating that for membrane surface activity of the small GTPase, the amphipathic helix is required. Next, we investigated the contribution of coatomer to membrane surface activity in this setup. Strikingly, simultaneous addition of coatomer and Arf1 leads to formation of morphologically distinct tubular membrane structures that are shorter than those generated by Arf1 in the absence of coatomer (Fig. 1 B, bottom right).

We next sequentially added first Arf1 and then coatomer to a hydrated lipid surface (Video 2 and Fig. 1 C). The fine tubules formed after Arf1 addition (Fig. 1 C, b, arrows) became shortened a few seconds after addition of coatomer (Fig. 1 C, c and d, arrows). At the same time, novel shorter tubular structures arose (Fig. 1 C, c–e, arrowheads) that became predominant ~8 s after coatomer addition (Fig. 1 C, f). The observations shown so far indicate that there are two distinct activities on the membrane surface, one by Arf1 alone and a second one after the addition of coatomer: coatomer is able to remodel Arf1-induced membrane tubules.

As published previously, Arf1-GTP can form a dimer on the membrane (Beck et al., 2008), and its membrane surface activity in vitro depends on dimerization. A dimerization-deficient mutant, Arf1-Y35A, cannot induce tubules under these conditions either in the absence or the presence of coatomer and does not support COPI vesicle formation. Expression of the mutant Arf1-Y35A cannot rescue Arf1/2 deletion in yeast. However, Arf1-Y35A is capable of recruiting coatomer to membranes in a GTP-dependent manner (Beck et al., 2008).

The structures, which result from the addition of Arf1 and coatomer to lipid surfaces (as observed in Video 2 and Fig. 1 C), cannot be resolved at the level of light microscopy, and therefore, to dissect the contributions of Arf1 and of coatomer to membrane deformation, we used cryo-EM. Liposomes were incubated either with Arf1–wild type (wt) or Arf1-Y35A in the presence of ARNO, coatomer, and guanine nucleotides (Fig. 2 A). With Arf1-wt, we observed coated liposomal structures of quite homogeneous size, reflecting reconstituted COPI vesicles as expected (Fig. 2 A, left). The diameter of the free vesicles was 59 ± 3 nm, consistent with previous observations (Spang et al., 1998; Bremser et al., 1999). We also saw vesicles in the process of budding, in which the bud membrane had remained continuous with the donor liposome. The diameter of the buds was 61 ± 4 nm. No free

size equivalent to one Airy disk diameter. (B) Membrane surface activity of Arf1 and coatomer. Lipids containing the p23 lipopeptide were spotted on a glass surface and hydrated with buffer containing GTP and 50 nM of the exchange factor ARNO. The lipid surface was observed before (left) and after addition of 1 µM myristoylated Arf1-GDP (top right) or by coinjection of 1 µM Arf1 and 0.25 µM coatomer (cm; bottom right). (C) Dissecting membrane surface activities of Arf1 and coatomer. (a) Lipids containing the p23 lipopeptide were spotted on a glass surface and hydrated with buffer containing GTP and the exchange factor ARNO as described in this legend. The image was taken, and thereafter, Arf1 was added, and tubule formation was observed (Video 1). (b) 0.25 µM coatomer was added to the chamber, leading to an immediate and nonspecific loss of most tubular structures caused by capillary flow forces. One frame afterward (t = 0), remaining Arf1-generated tubules are depicted (arrows). (c–f) Images were taken at 2, 4, 6, and 8 s after the addition of coatomer. The rapid degradation of Arf1-generated tubules (arrows) was followed over time, whereas new tubular structures with a distinct morphology were generated in the presence of coatomer (arrowheads). Bars, 5 µm.

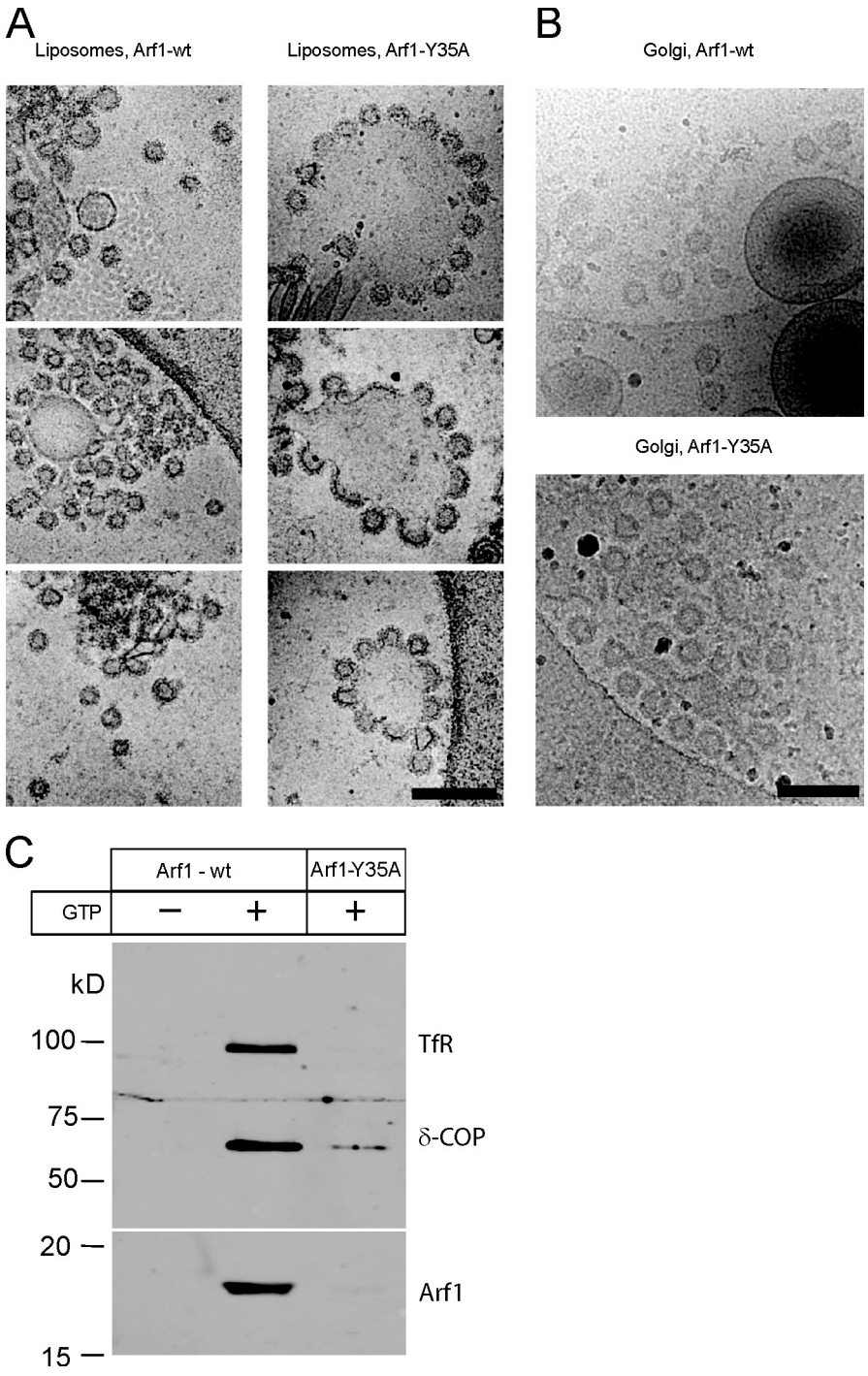

Figure 2. **COPI budding from synthetic liposomes and Golgi membranes analyzed by cryo-EM.** (A and B) Cryo-EM of membranes incubated with Arf1-wt or Arf1-Y35A in the presence of the guanine nucleotide exchange factor ARNO, coatomer, and GTPγS. Images show liposomes (A) and Golgi membranes (B). Bars, 200 nm. (C) Purification of reconstituted of COPI vesicles. Recombinant Arf1-wt or Arf1-Y35A was incubated with Golgi membranes in the presence of GDP or GTP as in Fig. 2 B. Vesicles were purified by sucrose density centrifugation. Samples in the vesicle fraction were analyzed by SDS-PAGE and Western blotting using antibodies against the membrane marker transferrin receptor (TfR) and against coatomer subunit δ-COP and Arf1.

vesicles or budding structures were observed in the absence of GTP. Strikingly, with dimerization-deficient mutant Arf1-Y35A, few distinct vesicles were found. Nevertheless, flower-like bud structures could be seen (Fig. 2 A, right), in which multiple budding events are taking place from individual liposomes. The bud membranes are still continuous with the liposomal membrane: scission has not taken place. The diameter of the buds is 63 ± 3 nm, the same as that for Arf1-wt. A similar result was obtained when Golgi-enriched membranes rather than liposomes were used (Fig. 2 B). These analyses show that despite the absence of membrane surface activity of Arf1-Y35A, formation of coated buds can still take place, implying a predominant role for coatomer in governing the shape of the vesicle. The shape could be governed directly by the geometry of polymerized coatomer and/or by coatomer positioning Arf1's myristoylated N-terminal helix to provide bud curvature. In summary, the Arf1-mediated membrane surface activity observed in Fig. 1 is not required to sculpt the shape of a nascent vesicle bud.

Evaluation of 148 coated vesicles or buds counted in the Arf1-wt liposome samples revealed that 22% of the structures unequivocally represent free vesicles, whereas with Arf1-Y35A,

only 2% were found separated from the liposomes (n = 120; Fig. 2 A). When Golgi membranes were used, increased background in the images caused by the membrane preparation makes it difficult to unambiguously quantify the number of vesicles that are released and that remain attached to donor membranes. We therefore quantitatively assessed vesicle release after isolation of COPI vesicles based on their buoyant density using Western blotting (Fig. 2 C). Free COPI vesicles were recovered in the presence of Arf1-wt in a GTP-dependent manner, as indicated by the presence of signals for transferrin receptor δ-COP and Arf1. In contrast, the monomeric mutant Arf1-Y35A did not support the reconstitution of free vesicles. These findings are consistent with our previous observations from in vitro Golgi budding assays, in which we could not reconstitute free COPI vesicles with the dimerization-deficient mutant Arf1-Y35A; only background amounts (<2%) of vesicles were recovered with Arf1-Y35A as compared with Arf1-wt (Beck et al., 2008). For further quantitative analysis of COPI reconstitutions and EM of isolated vesicles, see also Fig. 4 in this paper. Thus, although COPI buds are formed on Golgi membranes using either Arf1-wt or Arf1-Y35A (Fig. 2 B), only Arf1-wt releases those buds to yield free vesicles (Fig. 2 C).

The dimerization-deficient Arf1-Y35A can exchange GDP with GTP and recruit coatomer to membranes, yet the mutant cannot exert membrane surface activity and, therefore, cannot drive formation of free vesicles. Now, we find that coatomer recruited by Arf1-Y35A forms coated buds, as shown by cryo-EM (Fig. 2, A and B), but that vesicle scission does not take place, as shown by biochemical experiments (Fig. 2 C). Together, these observations indicate that vesicle production requires a combination of curvature-forming activity by coatomer, which defines the shape of the bud, and membrane surface activity contributed by Arf1. Furthermore, they assign a clear function for the membrane surface activity of Arf1 during scission. What are the molecular mechanisms that underlie this function?

Scission of a vesicle depends on dimerization of Arf1

As Arf1-Y35A fails to dimerize, we hypothesized that the formation of an Arf1-GTP dimer may be required to destabilize the membrane at the bud neck and allow fission. To challenge this hypothesis, we tested whether a forced dimerization of the Arf1-Y35A mutant by chemical cross-linking would restore scission activity, as might be expected if dimerization was the only defect of this mutant. To this end, the single cysteine residue of both Arf1 and Arf1-Y35A was replaced with serine, and the C-terminal lysine was substituted with cysteine, yielding Arf1-C159S-K181C and Arf1-Y35A-C159S-K181C (from here on referred to as Cys-wt and Cys-Y35A, respectively). Published work has demonstrated that adding a Cys residue to the C terminus of the small GTPase is permissive for Arf1 function (Manneville et al., 2008).

These variants were then analyzed in a liposomal binding assay. Liposomes were isolated by centrifugation and analyzed for their content of Arf1 variants by Western blotting. Arf1-wt and Cys-wt were found to bind to membranes in a GTP-dependent manner and to a comparable extent (Fig. 3 A, compare lane 2 with 4 and lane 6 with 8). Note that the faster migrating band in the input lanes reflects myristoylated Arf1, and the top band reflects the nonmyristoylated form of Arf1, which fails to bind membranes and, therefore, does not show up in the liposomal fraction. Thus, exchange of Cys 159 to Ser and Lys 181 to Cys does not compromise Arf1's specific binding to membranes. In the case of the mutant Cys-Y35A, no binding was observed (Fig. 3 A, lanes 10 and 12). This was expected, as it was shown previously that binding to liposomal membranes of the dimerization-deficient Arf1-Y35A variant required the presence of coatomer (Beck et al., 2008).

Next, the Cys variants were dimerized by reaction with a homobifunctional SH-reactive reagent, bismaleimidohexane (BMH), and the extent of cross-linking was analyzed by SDS gel electrophoresis. Both proteins were dimerized efficiently and to a similar extent, as shown by Coomassie staining in Fig. 3 B, in which the Arf1 dimers migrate with an apparent molecular mass of ∼37 kD.

A well-established static light scattering assay (Bigay and Antonny, 2005) was used to monitor membrane dynamics of Arf1-wt, Arf1-Cys, cross-linked Arf1-Cys (cl-Arf1-Cys), and coatomer. As depicted in Fig. S2, nucleotide exchange of Arf1-wt and Cys-wt is comparable. Cl^- Cys-wt shows a faster rate of GTP loading, probably because of the increased membrane avidity of the dimer. Arf GTPase-activating protein (ArfGAP)–mediated GTP hydrolysis is comparable for all three proteins; however, the dimeric construct leaves the membrane with slightly slower kinetics, likely caused by the need of hydrolyzing two nucleotides in one molecule (Fig. S2).

To study the membrane-binding properties of the dimerized proteins, chemically cross-linked Cys-wt was tested for membrane binding as before analyzed by floatation, as shown for the non–cross-linked Arf1 variants earlier in this paper. As depicted in Fig. 3 C, chemical cross-linking of Cys-wt results in efficient membrane binding comparable with that of Arf1-wt (Fig. 3 C, compare the ratio of lanes 3 and 4 with the ratio of lanes 7 and 8). The larger fraction of bound cl-Cys-wt likely reflects increased avidity resulting from dimerization. Membrane avidity was increased by dimerization to an extent that led to some binding even in the absence of GTP (Fig. 3 C, lane 6). Most remarkably, the dimerization-deficient Arf1 variant Cys-Y35A, upon dimerization by chemical cross-linking, gains capability to bind to membranes even in the absence of a coatomer, as shown in Fig. 3 C (lane 12). Again, some binding of chemically cross-linked Cys-Y35A is observed in the absence of GTP (Fig. 3 C, lane 10).

The experiments in Fig. 2 show a scission arrest for monomeric Arf1-Y35A when compared with Arf1-wt. We next analyzed whether chemically cross-linked Cys-Y35A dimers can support the scission reaction, i.e., form free COPI vesicles. Cys-wt and Cys-Y35A were chemically cross-linked and incubated with Golgi membranes and the coatomer in the presence or absence of GTP followed by isolation of COPI vesicles based on their buoyant density and analysis by Western

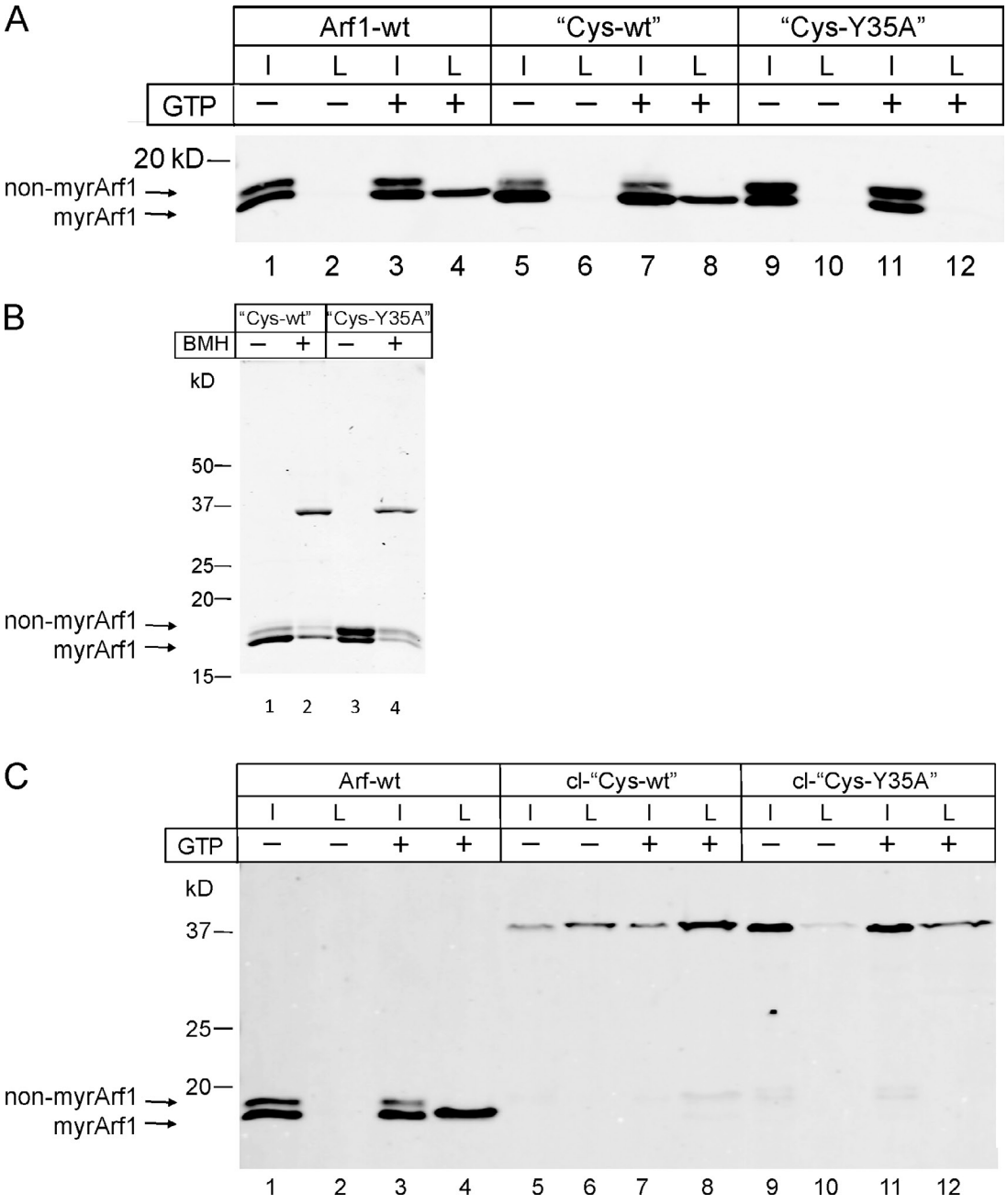

Figure 3. **Binding of Arf1 and Arf1 variants to synthetic liposomes.** (A) Comparison of the binding ability of Arf1-wt, Cys-wt, and Cys-Y35A to synthetic liposomes in the absence and presence of GTP. Arf1 variants were mixed with liposomes to a final concentration of 1.5 µM protein and 0.5 mM lipid in the presence of ARNO in a total volume of 100 µl. After 15 min of incubation at 37°C with or without 1 mM GTP, the samples were floated to an interface between 25 and 0% (wt/vol) sucrose. 10% of the collected liposomal fractions was compared with 5% of the input and analyzed for the presence of Arf1 and the Arf1 variants by SDS-PAGE and Western blotting, respectively. non-myrArf1, nonmyristoylated Arf1; myrArf1, myristoylated Arf1. (B) Cross-linking of the Cys variants using BMH. Purified Arf1 protein was mixed with BMH in a molar ratio of 2:1 and incubated for 1 h at RT. Thereafter, the cross-linking reaction was quenched by the addition of DTT and analyzed by SDS-PAGE and Coomassie staining. (C) Analysis of the binding ability of cross-linked Cys-wt (cl-Cys-wt) and Cys-Y35A (cl-Cys-Y35A) to synthetic liposomes in the absence and presence of GTP. The assay was performed as outlined in A. I, input; L, liposome-bound fraction.

blotting (Fig. 4 A) and EM (Fig. 4 B; Weimer et al., 2008; Beck et al., 2009a). Arf1-wt served as a positive control (Fig. 4 A, lane 4). Like Arf1-Y35A (Fig. 2 C), the non–cross-linked variant Cys-Y35A failed to produce free vesicles (Fig. 4 B and Fig. S3). Strikingly, upon dimerization by chemical cross-linking, this mutant gives rise to efficient vesicle formation to an extent comparable with that of chemically cross-linked Cys-wt, as shown in Fig. 4 A (lanes 12 and 8).

To control for possible effects of the Cys mutation and chemical cross-linking on Arf1 function, reconstituted COPI vesicles were probed by Western blotting for cargo and noncargo (excluded) markers (Fig. S4). We find uptake of α-mannosidase II in all COPI vesicle fractions independent of the Arf1 used, indicating that this Golgi resident enzyme is taken up into the vesicles as expected. As an excluded protein, we analyzed $G\alpha_s$, which was shown previously to localize to the Golgi but is excluded from COPI vesicles

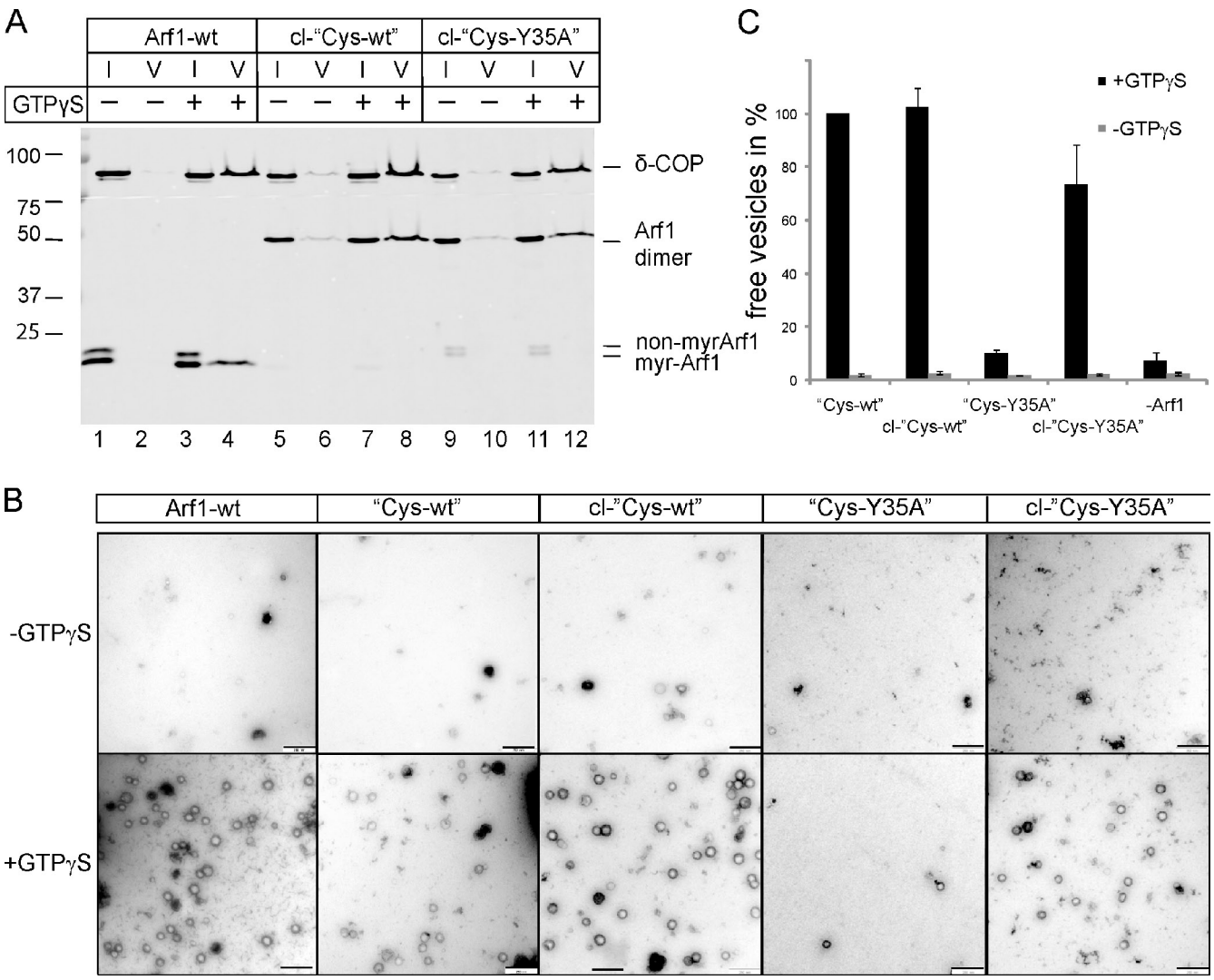

Figure 4. **Dimerization of Cys-Y35A restores its ability to generate COPI-coated vesicles from Golgi membranes.** (A) COPI-coated vesicles were reconstituted from Golgi membranes using Arf1-wt, cross-linked Cys-wt (cl-Cys-wt), or cross-linked Cys-Y35A (cl-Cys-Y35A) in the presence of GTPγS and purified coatomer. Vesicles were purified via sucrose density centrifugation. 1% of input (I) and 50% of vesicle (V) fractions were analyzed by SDS-PAGE and Western blotting against δ-COP and Arf1. Non-myrArf1, nonmyristoylated Arf1; myr-Arf1, myristoylated Arf1. (B) Purified vesicles were analyzed by negative staining EM. Bars, 250 nm. (C) Quantification of vesicle formation: 14 image sections of 3-μm^2 size were randomly chosen, and the number of vesicles was counted. Error bars represent the standard deviation of the mean of three independent experiments. Molecular masses are given in kilodaltons.

(Helms et al., 1998). As a result, with all Arf1 variants, we find efficient exclusion of $G\alpha_s$. Thus, neither the Cys mutation nor its cross-linking had detectable influence on cargo uptake or exclusion.

Reconstituted vesicles were further analyzed by negative stain EM (Fig. 4 B), and the data were quantified (Fig. 4 C). Although in the non–cross-linked Cys-Y35A sample, there was a background amount of ∼90 vesicles per 42 meshes (a number similar to that obtained in negative controls, in which no Arf1 was added and in which a few vesicles are formed because of residual Arf1 present in the Golgi preparations as shown in Fig. 4 C), after cross-linking, ∼700 vesicles were counted in the same field size. This reflects an efficiency of vesicle formation of ∼70% when compared with dimerized Cys-wt. These results show that the arrest in vesicle scission caused by the Y35A mutation can be rescued by chemical cross-linking–induced dimerization. Dimerization of Arf1 is therefore required for membrane scission during vesicle formation.

How is this dimerization of the small GTPase linked to the scission reaction? To address this mechanism at a molecular level, we studied the interactions of Arf1 with a coatomer that shapes the membrane to form a bud.

Anchoring of Arf1 in its overlaying scaffold of coatomer

wt Arf1-GTP is stably anchored in the shell of the budding vesicle by specific interactions with various subunits of coatomer, as indicated by site-directed photolabeling experiments (Zhao et al., 1997, 1999; Sun et al., 2007). Therefore, we assessed whether Arf1-wt and Arf1-Y35A adopt the same conformation and interactions within the coat. To this end, Arf1 variants were generated containing a photoreactive benzophenone derivative of phenylalanine (*p*-benzoyl-L-phenylalanine [Bp]) at position I49 or Y167, previously shown to contact coatomer at different sites. Upon UV irradiation, covalent bonds will be formed between the

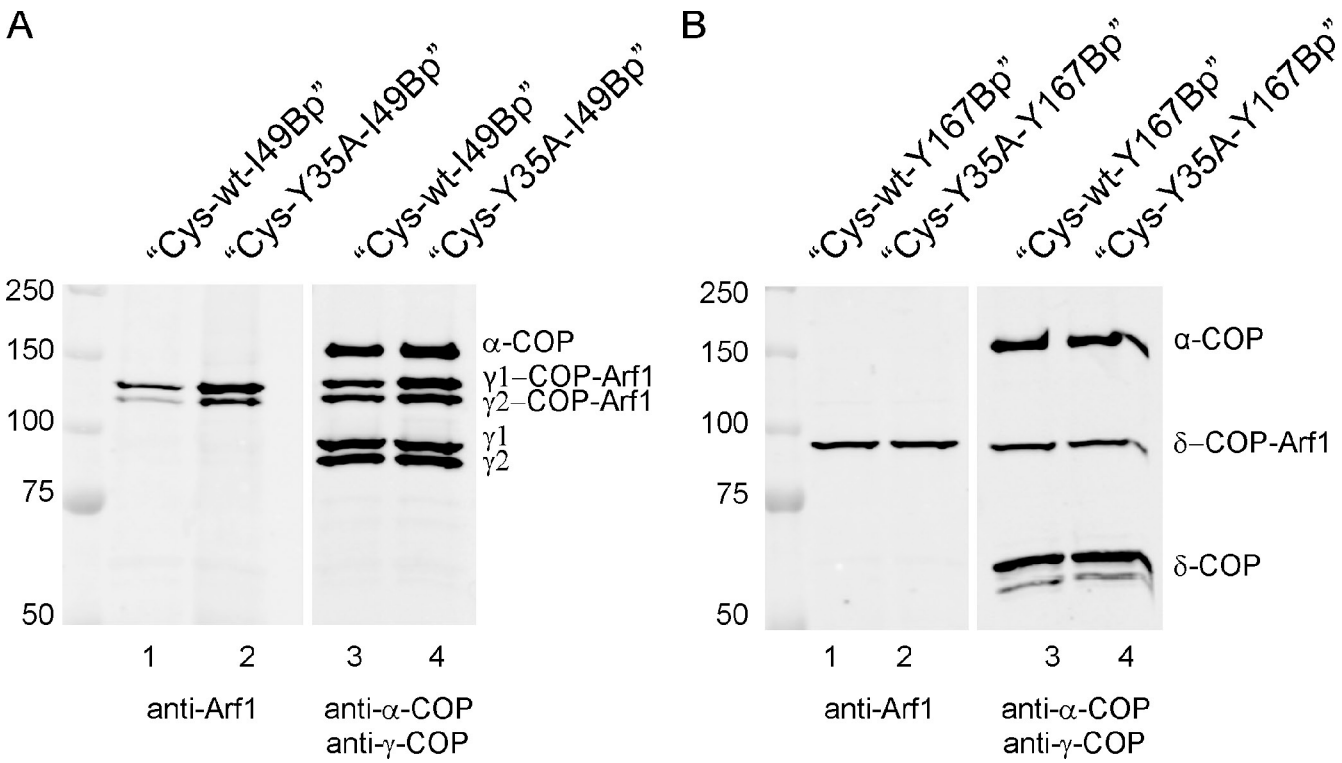

Figure 5. **Interactions of Arf1 with coatomer probed by site-directed photo–cross-linking.** Arf1 variants with a photolabile amino acid residue in either position 49 or 167 were prepared as described in Materials and methods and used for coatomer recruitment to Golgi membranes. Membranes were separated by centrifugation and UV irradiated followed by SDS-PAGE and Western blotting. (A) Analysis of photo–cross-link products with the photolabile amino acid derivative in position 49. Lanes 1 and 2 show Cys-wt and Cys-Y35A, respectively, decorated with anti-Arf1 antibodies. Lanes 3 and 4 show samples as in lanes 1 and 2 decorated with anti–γ-COP and, as a control, with anti–α-COP antibodies. (B) Analysis of photo–cross-link products with the photolabile amino acid derivative in position 167. Lanes 1 and 2 are decorated with anti-Arf1 antibodies, and lanes 3 and 4 are decorated with anti–δ-COP and anti–α-COP antibodies. For details of preparation of site-directed photolabile Arf1 derivatives see Materials and methods. Molecular masses are given in kilodaltons.

photoactive amino acid residue and nearby residues across interaction interfaces. These photolabile Arf1 variants were incubated with Golgi membranes and coatomer. Membranes were isolated and UV irradiated to generate cross-links of the photolabile Arf1 variants with coatomer subunits within the recruited coat. The samples were analyzed by Western blotting with antibodies directed against Arf1 and against the respective COPI subunits.

A photo–cross-link is observed between position 49 of both Arf1-wt-I49Bp and Arf1-Y35A-I49Bp and γ1- and γ2-COPs (Fig. 5 A) and between position 167 of both Arf1-wt-Y167Bp and Arf1-Y35A-Y167Bp and δ-COP (Fig. 5 B). The corresponding bands in both cases are of similar intensity. A cross-link, e.g., between α-COP with photolabile Arf1 variants, was not observed, in accordance with Zhao et al. (1999) and Sun et al. (2007). These results establish that the point mutation in Arf1-Y35A leaves intact the known interactions of coatomer with the small GTPase and indicate that it is missing the interface of Arf1-Y35A with its kin rather than its interfaces with coatomer, which impairs membrane fission.

Effects of dimerization-deficient Arf1 in vivo

To analyze the effect of dimerization deficiency of Arf1 in a living cell, cells were microinjected with cDNAs encoding Arf1 variants. Because the effects of Arf1-Y35A can be rescued by endogenous Arf1-wt, we also used GTP-locked forms of Arf1-wt and Arf1-Y35A (Dascher and Balch, 1994). As expected, microinjection of Arf1-wt or Arf1-Y35A was not lethal and did not show alterations in subcellular localization of Golgi markers (unpublished data). As a striking result, we observed cell lethality 4 h after injection of Arf1-Y35A-Q71L, however, not of Arf1-Q71L. We analyzed cells 2 h after microinjection. In immunofluorescence analyses with antibodies directed against attached and integral Golgi membrane markers, as well as against coatomer, we observed that Arf1-Y35A-Q71L (and not Arf1-Q71L) causes loss of cis-peripheral Golgi proteins (GM130; Fig. S5 A) and, to a lesser extent, GMAP-210 (not depicted). The integral Golgi protein giantin remains unaffected, whereas a reduced Golgi localization of β1,4 galactosyltransferase (GalT) is observed for both Arf1-Y35A-Q71L and Arf1-Q71L. With antibodies directed against coatomer 2 h after injection of Arf1-Y35A-Q71L, a more condensed Golgi-like pattern is seen compared with Arf1-Q71L.

Analysis by EM of thin sections 2 h after injection is shown in Fig. S5 B. Injection of Arf1-Q71L gave rise to an accumulation of vesicular structures (Fig. S5 B, A–D) as expected (Tanigawa et al., 1993) and left the morphology of the stacked Golgi cisternae intact. In the case of Arf1-Y35A-Q71L, we were unable to observe any Golgi stacks within the injected cells (Fig. S5 B, E–H). Thus, the condensation observed with coatomer as a Golgi marker in immunofluorescence is reflected by a disappearance of stacked cisternae.

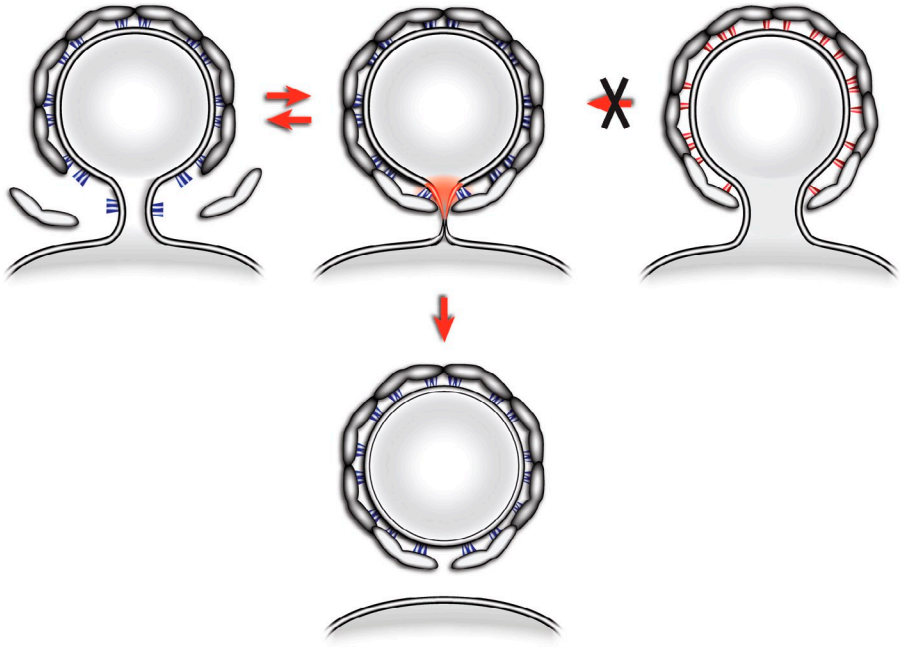

Figure 6. **A model for Arf1-mediated membrane separation.** The process of COPI budding and fission is depicted. Arf1 is recruited to the neck of a growing bud and stabilized in this location by coatomer (Arf1-Y35A in red; Arf1-wt in blue). As the growing bud becomes completed, the local membrane curvature creates an unfavorable situation for the insertion of the myristoylated amphipathic helix of Arf1. If Arf1 is enforced in this area by its multiple interactions with the covering network of polymerized coatomer, this will lead to local strain in the membrane (in red). The resulting metastable intermediate can then be relaxed in an irreversible manner by membrane separation. The resulting shell of polymerized coatomer is drawn with a gap because any possible contribution to membrane fission by closing this gap is not addressed here.

Together, these data are compatible with a requirement in vivo for dimeric Arf1. The dramatic phenotype in vivo is likely because Arf1 not only is involved in the formation of COPI vesicles but also of AP1, AP3, AP4, and GGA (Golgi localized, γ-adaptin ear containing, Arf binding) carriers.

Discussion

The results presented in this paper establish that the point mutation in Arf1-Y35A leaves Arf1's known coatomer interactions intact and permits recruitment of coatomer to membranes and formation of a bud but leads to a block in scission. At the molecular level, we show that this fission arrest results from a loss of the propensity of the small GTPase to dimerize upon activation. By forcing dimerization through chemical cross-linking of Arf1-Y35A, the scission arrest of the mutant can be overcome. Dimerization of Arf1 is therefore required for separation of a COPI vesicle from its donor membrane.

We note that direct cryo-EM of the reconstituted reaction shows that coated buds are formed by both Arf1-wt and Arf1-Y35A (Fig. 2), suggesting that only the Arf1-wt can yield released vesicles. Biochemical separation by sucrose gradient purification confirms that only Arf1-wt and not Arf1-Y35A yields released vesicles. Because both Arf1-wt and the mutant are treated in the same manner, these observations argue strongly against mechanical manipulation or physical perturbation as the cause of vesicle release in our observations.

A model for membrane scission

The production of COPI-coated vesicles likely results from an interplay between a scaffold mechanism, in which coatomer drives bending of the membrane to form a COPI bud, and an independent mechanism, in which shallow insertion of the amphipathic helix of Arf1 into the membrane exerts a membrane surface activity (McMahon and Gallop, 2005; Pucadyil and Schmid, 2009). To build the initial vesicular shell, Arf1 binds coatomer via several COPI subunits (Zhao et al., 1997, 1999; Sun et al., 2007), the membrane via its myristoylated α helix (Antonny et al., 1997), and another Arf1 monomer via the dimerization interface (Beck et al., 2008). Arf1 will therefore be linked tightly to both the coat above and the phospholipid bilayer below. In the region of a bud's neck, membrane areas exist with positive and negative curvature (Drin and Antonny, 2005). Activated Arf1 will most stably be bound to regions where the membrane is positively curved (with less tightly packed outer leaflet lipids) perpendicular to the inserted amphipathic helix. Insertion of the helix in an orientation perpendicular to negative curvature (where lipids are more tightly packed) would create an energetically unfavorable state.

The binding of activated Arf1 to the membrane could contribute to scission in two conceptually different ways. In the first, Arf1 could be arranged to form a ring around the bud neck, with the helices oriented perpendicular to the neck. This model has been proposed for Sar1 (Drin and Antonny, 2005) and requires a specific arrangement of the small GTPase at the bud neck, different to that within the spherical bud coat. In a second model, depicted in Fig. 6, Arf1 is incorporated in an arrangement stable only in the spherical surface of the bud (Fig. 6, Arf1-wt in blue and Arf1-Y35A in red). During budding, Arf1 and coatomer are recruited at the edge of the growing coat, a region that has increasing negative curvature as the bud becomes more complete. Enforcement by multiple coatomer interactions of Arf1 dimers in these negatively curved regions (where, in addition, the Arf1 GTPase-activating enzyme ArfGAP1 is excluded [Bigay et al., 2003] and, therefore, less Arf1 will be removed from the membrane [Ambroggio et al., 2010]), with an unfavorable orientation of the amphipathic helix (Fig. 6, regions highlighted in red), would induce

increasing strain in the membrane. This could be released by scission, providing a basic mechanism for membrane separation. Destabilization of the Arf1 dimerization interface through the Y35A mutation would reduce the stability with which Arf1 is anchored within the membrane. Although the interaction of monomeric Arf1-Y35A molecules with the covering scaffold of polymerized coatomer is intact, the binding energy between two Arf1 molecules is missing, and therefore, the force is correspondingly lower by which Arf1 is kept in energetically unfavorable zones of negative curvature. The resulting lack of membrane strain would lead to a block in scission. At this point, we cannot exclude the possibility that dimerization occurs selectively during the final constriction step at the vesicle neck.

The conclusions presented here are based on in vitro observations in a defined liposomal system and on Golgi membranes. Combined with the known inability of Arf1-Y35A to rescue Arf-deficient yeast (Beck et al., 2008), these results provide compelling evidence that dimerization of Arf1 represents a key mechanism for scission in the COPI system. Likewise, in the mammalian living cell, dimerization deficiency of Arf1 locked in its activated state is lethal and causes severe disruption of Golgi architecture (Fig. S5). Arf1 might have a similar role in scission during the formation of related adaptor-dependent vesicles. Indeed, direct interactions of Arf1 with corresponding subunits of clathrin adaptor complexes 1 (Stamnes and Rothman, 1993; Austin et al., 2000, 2002), 3 (Austin et al., 2002), and 4 (Boehm et al., 2001) and the GGA coat (Puertollano et al., 2001) have been previously described. In this context, it is of note that the dimerization-deficient mutant Arf1-Y35A was also able to recruit to membranes the adaptor protein complex I (Beck et al., 2008). Furthermore, the finding that Sar1p, like Arf1, exerts membrane surface activity, which is required for the release of COPII buds (Lee et al., 2005), suggests a general role of small GTPases in vesicle formation and release. It will be of interest in the future to analyze whether, in the COPII system, oligomerization of Sar1p (Long et al., 2010) provides the molecular mechanism that underlies the process of membrane separation. In vivo, additional factors, lipids, and proteins, such as ArfGAPs, brefeldin A ADP-ribosylated substrate, and others, were suggested to contribute to vesicle release (Beck et al., 2009b; Hsu et al., 2009).

In summary, we were able to dissect cooperating contributions to vesicle budding and fission of Arf1 and coatomer. On the one hand, coatomer recruited by Arf1 is needed to form the curvature of a COPI bud, and on the other hand, dimeric Arf1's membrane surface activity in cooperation with coatomer drives membrane separation.

Materials and methods

Proteins

Reagents for expression of site-directed photolabile proteins in *Escherichia coli* were provided by P.G. Schultz (The Scripps Research Institute, La Jolla, CA). Antibodies directed against $G\alpha_s$ were provided by B. Nürnberg (Universitätsklinikum Tübingen, Tübingen, Germany). The cDNAs for the following Arf1 variants were generated by site directed mutagenesis: Arf1Y35A (Beck et al., 2008), Arf1-C159S-K181C (Cys-wt), Arf1-Y35A-C159S-K181C (Cys-Y35A), Arf1-I49Amber-C159S-K181C (Cys-wt-I49Bp), Arf1-Y35A-I49Amber-C159S-K181C (Cys-Y35A-I49Bp), Arf1-Y167Amber-C159S-K181C (Cys-wt-Y167Bp), and Arf1-Y35A-Y167Amber-C159S-K181C (Cys-Y35A-Y167Bp). Full-length myristoylated human Arf1-wt and the Cys variants were recombinantly expressed and purified as described previously (for photolabile proteins see Photo–cross-linking experiments; Franco et al., 1996). In short, human Arf1 and yeast *N*-myristoyltransferase were coexpressed in *E. coli* supplied with BSA-loaded myristate. Cell lysates were subjected to 35% ammonium sulfate, and the precipitate was enriched in myristoylated Arf1 was further purified by DEAE ion exchange. After cell lysis and ultracentrifugation, Arf1-Y35A was subjected to a 35% ammonium sulfate precipitation and centrifuged, and the supernatant was bound to a phenyl-Sepharose high performance column (Pharmacia Biotech) and developed with a descending gradient from 35 to 0% ammonium sulfate in 20 mM Tris-HCl buffer, pH 8.0, and 1 mM $MgCl_2$ at RT. Eluted fractions were analyzed by immunoblotting with the anti-Arf1 antibody, pooled, concentrated in spin-column filters with a 10-kD cutoff (Millipore), and subsequently, purified by gel filtration on a Superdex 75 (GE Healthcare). Fractions of interest were pooled and concentrated.

Coatomer was purified from rabbit liver (Nickel and Wieland, 2001). His-tagged ARNO was expressed in *E. coli* and purified by Ni-nitrilotriacetic acid chromatography (Chardin et al., 1996).

Chemical cross-linking of Arf1 proteins

A protein concentration of 100 µM or higher was used for chemically cross-linking GDP-loaded Cys-wt or Cys-Y35A in a molar ratio of 2:1 with the homobifunctional bismaleimide cross-linker BMH (Thermo Fisher Scientific) in 20 mM Hepes buffer at pH 7.0 according to the manufacturer's protocol. GDP-loaded Arf1-wt is not cross-linked under these conditions. Subsequently, the cross-linking reaction was quenched with DTT at a final concentration of 100 mM.

Preparation of Golgi membranes and liposomes

Golgi membranes were purified from rat liver homogenates (Tabas and Kornfeld, 1979). Lipids were purchased from Avanti Polar Lipids, Inc. except for phosphatidic acid, which was obtained from Sigma-Aldrich. Lipids were derived from natural sources. Golgi-like liposomes were prepared containing 1 mol% phosphatidylinositol-4,5-bisphosphate ($PI(4,5)P_2$) and 2 mol% p23 lipopeptide, which was synthesized according to Nickel and Wieland (2001). Size selection was performed by extrusion through 400-nm polycarbonate filter membranes (Avestin).

GUVs preparation and imaging

GUVs were generated by the electroswelling method with a Golgi-like lipid mix supplemented with 3 mol% p23 lipopeptide, 1 mol% ($PI(4,5)P_2$), 0.1 mol% 1,2-dioleoyl-*sn*-glycero-3-phosphoethanolamine-*N*-biotinyl, and 0.5 mol% 1,2-dipalmitoyl-*sn*-glycero-3-phosphoethanolamine-*N*-lissamine rhodamine B sulfonyl in 300 mM sucrose. Lab-Tek chambered cover slides were preincubated with 1 mg/ml BSA/BSA-biotin (100:1; mol/mol) for 30 min, rinsed three times with HKM buffer (50 mM Hepes-KOH, pH 7.4, 150 mM KCl, and 1 mM $MgCl_2$) and subsequently with 0.1 mg/ml avidin, and rinsed again three times with HKM buffer.

For visualizing of Arf1-induced tubules, 20 µl of the GUV preparation was transferred into a coated Lab-Tek chambered cover slide and incubated after sequentially adding 3.5 µM Arf1-wt, 0.4 µM ARNO, and 1 mM GTP in a total volume of 200 µl for 10 min at RT. Confocal images were acquired with a laser-scanning microscope (510 Meta; Carl Zeiss) equipped with a 543-nm HeNe laser and a 560 low pass filter.

Arf1-induced tubulation of membrane sheets

A system similar to that previously described in Roux et al. (2006) was used. A chamber of approximately 30 µl was built between two microscope slides with two layers of parafilm as a spacer. Golgi-like lipids containing 1 mol% $PI(4,5)P_2$ and 2 mol% p23 lipopeptide (Bremser et al., 1999) were spotted on the glass surface, and the solvent ($CHCl_3$) was evaporated. The lipids were hydrated in the presence of nucleotide with 20 µl assay buffer (25 mM Hepes-KOH, pH 7.4, 150 mM KCl, 1 mM DTT, and 1 mM GTP or GDP). Then, protein samples were sequentially added to give final concentrations of 1 µM Arf1, 50 nM ARNO, and 250 nM coatomer, and membrane morphology was observed at RT in a phase-contrast light microscope (Axiomat 200M; Carl Zeiss) using a Plan Apochromat 100× objective (NA = 1.4). Images were captured with a camera (AxioCam MRm; Carl Zeiss). The imaging software used was Axiovision (Carl Zeiss) and ImageJ (National Institutes of Health). Real-time recordings are appended to supporting information.

Cryo-EM

COPI reconstitution assays were performed with 20 µg liposomes in the presence of 10 µg Arf1-wt (or Arf1-Y35A), 3 µg ARNO, 250 µM GTPγS, 1 mM $MgCl_2$, 20 µg coatomer, and 100 mM NaCl in 50 mM Hepes, pH 7.5. Alternatively, 20 µg Golgi-enriched membrane was used instead of synthetic liposomes. Reactions were incubated for 30 min at 37°C and transferred to 4°C during preparation for EM. Samples were vitrified by plunge freezing on holey carbon grids. Grids were imaged using an electron microscope (Tecnai F30; FEI) equipped with a 4,000 × 4,000–pixel charge-coupled device camera (Eagle; FEI) and operated at 300 kV. Data were collected at between 4 and 6–µm underfocus 39,000 magnification, resulting in a pixel size of 0.3 nm at the specimen level. Dose per image was 15–25 $e^{-}Å^{-2}$.

Negative staining EM

A carbon-coated grid was put on top of a 5-µl droplet of purified COPI vesicles. After 10 min of adsorption at RT, proteins were fixed by putting the grid onto a 20-µl droplet of 1% glutaraldehyde in assay buffer (25 mM Hepes-KOH, pH 7, and 2.5 mM Mg-acetate), washed three times with 20 µl assay buffer each, and incubated for 5 min in 0.05% tannic acid. All these steps were performed at RT. Afterward, the sample was washed four times with 20 µl of water. Then, staining was performed with 0.4% uranyl acetate in 1.8% methylcellulose for 10 min on ice.

EM of thin sections of cells

HeLa cells were grown on gridded coverslips (CELLocate; Eppendorf) to ∼30% confluency and microinjected with plasmids encoding either GFP-tagged Arf1-Q71L-Y35A double mutant or the Arf1-Q71L single mutant as a control (see Immunofluorescence imaging of Arf1 variants in HeLa cells for details on microinjection). 2 h after injection, transfected cells were identified by fluorescent light microscopy, and their position on the gridded coverslip was recorded and mapped. Cells were chemically fixed for 30 min at RT with 2.5% glutaraldehyde in 0.1 M Na-cacodylate buffer, postfixed on ice with 2% OsO_4 in the same buffer, washed, dehydrated in a graded series of ethanol, and embedded in their in situ orientation in epoxy resin (Glycidether 100; Carl Roth).

70-nm-thin sections of mapped areas of interest were cut (from the bottom to the top of the cells) with a microtome (Ultracut UCT; Leica) and a diamond knife, placed on copper grids (2 × 1–mm slot), and poststained with Reynold's lead citrate. Profiles of injected cells were identified and examined with a transmission electron microscope (operated at 100 kV; Morgagni; FEI) equipped with a 1,000 × 1,000–pixel charge-coupled device camera.

Membrane-binding assay

Flotation experiments were performed in HKM buffer (Hepes-KOH, pH 7.4, 120 K-acetate, and 1 mM $MgCl_2$) containing 100 mM DTT in a total volume of 100 µl using 1.5 µM Arf1, 0.05 µM guanine nucleotide exchange protein ARNO, and 0.5 mM liposomes in the presence or absence of 1 mM GTP. After incubation for 15 min at 37°C, sucrose was added to a final concentration of 30%. The samples were overlaid with 300 µl of 25% sucrose and 50 µl HKM buffer and centrifuged for 1 h at 250,000 *g* in a rotor (SW60Ti; Beckman Coulter). 10% of the top fraction was analyzed for bound proteins by SDS-PAGE and Western blotting.

Vesicle budding assay

To generate COPI-coated vesicles, 125 µg of salt-washed Golgi membranes (Beck et al., 2009a) were mixed with 5 µg myristoylated Arf1, 40 µg coatomer, and 0.1 mM GTPγS (or 1 mM GTP) in assay buffer (25 mM Hepes-KOH, pH 7, 2.5 mM Mg-acetate, and 100 mM DTT) in a total volume of 250 µl. After incubation for 10 min at 37°C, the salt concentration was raised to 250 mM KCl, and the sample was centrifuged at 12,000 *g* for 10 min. The supernatant containing COPI vesicles was loaded on top of two sucrose cushions (5 µl of 50% and 50 µl of 37% sucrose) and centrifuged for 50 min at 100,000 *g* in a rotor (SW60Ti). COPI-coated vesicles were concentrated at the interphase between 50 and 37% sucrose. 2% of the input and 50% of the isolated vesicle fraction were analyzed by SDS-PAGE and Western blotting.

Photo–cross-linking experiments

For expression of photolabile Arf1 variants, the plasmids pBad-tRNA-hArf mutant-TAG and pBK-pAFRS were cotransformed into DH10B *E. coli* strains (Wang et al., 2001). The cells were grown in 2× YT (yeast extract and tryptone) medium containing 30 µg/ml kanamycin and 25 µg/ml tetracycline until OD_{600} = 0.6. After a washing step with M9 medium, the cells were transferred in glycerol minimal medium and leucine medium containing the appropriate antibiotics, 1 mM myristic acid, and 1 mM Bp. Protein expression was induced by the addition of 0.5% arabinose. Cells were grown for 22 h at 27°C, harvested by centrifugation, and lysed in 25 mM Tris-HCl, pH 7.2, 50 mM KCl, 1 mM DTT, and protease inhibitor cocktail (Roche). Lysates were cleared by centrifugation for 30 min at 10,000 *g*, and the supernatants were centrifuged for 60 min at 100,000 *g*. The cell lysates so obtained were stored at −80°C. 5 µg photolabile Arf1 variants and 25 µg Golgi membranes were incubated in assay buffer (25 mM Hepes-KOH, pH 7.2, 25 mM Mg-acetate, 100 mM DTT, and 200 mM sucrose) in the presence or absence of 100 µM GTPγS for 5 min at 37°C. Coatomer was added, and the sample was incubated for additional 15 min at 37°C. Golgi membranes were recovered by loading the sample onto a 15% sucrose cushion followed by a 30 min centrifugation at 16,000 *g* (4°C). The pellet was resuspended in assay buffer and irradiated at 366 nm for 40 min. Samples were analyzed by SDS-PAGE and Western blotting.

Static light scattering

Nucleotide exchange and hydrolysis on chemically cross-linked Arf1 was measured as previously described (Bigay and Antonny, 2005). Golgi-like liposomes containing 1 mol% $PI(4,5)P_2$ and 2 mol% p23 lipopeptide were monitored over time in 25 mM Hepes-KOH, pH 7.4, 150 mM KCl, and 1 mM $MgCl_2$ by using a spectral photometer (FP-6500; Jasco). 1 µM Arf1-wt, 1 µM Arf1 Cys-wt, or 0.5 µM chemically cross-linked cl-Cys-wt was added followed by 1 mM GTP and 0.2 µM coatomer. Nucleotide exchange was started by the addition of 2 mM EDTA (after 60 s) to chelate Mg^{++}. After nucleotide exchange, the Mg^{++} concentration was raised to 5 mM, and 25 nM ArfGAP2 was injected (after 640 s).

Immunofluorescence imaging of Arf1 variants in HeLa cells

The bicistronic plasmid for the expression of EGFP (used as a marker to identify the injected cells) and coding for the different Arf1 variants were microinjected at the concentration of 500 ng/µl into the nucleus of HeLa Kyoto cells using a microinjector (Transjector 5246 and Micromanipulator 5171; Eppendorf). The cells were fixed with 3% PFA 2 h thereafter. For immunostainings, we used standard procedures, diluting the antibodies in PBS containing 10% FCS and 0.1% saponin. Primary antibodies used were rabbit polyclonal giantin (Abcam), mouse monoclonal GM130 (BD), mouse monoclonal GalT (Cellmab), and rabbit polyclonal β′ Cop (raised in our laboratory with standard procedures). Secondary antibodies used were Alexa Fluor 568–conjugated anti–mouse and Alexa Fluor 568–conjugated anti–rabbit (Invitrogen). Confocal sections were acquired every 300 nm across the entire volume of the cells using a 53× Plan Apochromat oil immersion objective (NA = 1.4) on a laser-scanning confocal microscope (SP5; Leica). Maximum projections of the image stacks were generated with the SP5 analysis software.

Online supplemental material

Fig. S1 shows membrane binding of His-tagged proteins to Ni-liposomes. Fig. S2 shows nucleotide exchange and hydrolysis by chemically cross-linked Arf1 variants. Fig. S3 shows COPI reconstitutions from Golgi membranes using non–cross-linked Arf1-Cys variants. Fig. S4 shows COPI reconstitutions from Golgi membranes with Arf1-Cys variants to analyze cargo markers included in or excluded from the vesicles. Fig. S5 shows in vivo analysis of dominant-negative Arf1-Q71L or Arf1-Y35A-Q71L in HeLa cells by single-cell thin-section EM and immunofluorescence microscopy. Video 1 shows analysis of membrane surface activity of NΔ17-Arf1. Video 2 shows analysis of membrane surface activity upon addition of Arf-wt and membrane remodeling by subsequent addition of coatomer. Online supplemental material is available at http://www.jcb.org/cgi/content/full/jcb.201011027/DC1.

We thank Michael Brunner for helpful discussions and suggestions, Ingrid Meissner, Inge Reckmann, and Andrea Hellwig for technical assistance, Marco Faini for helpful discussions, and Dan Cassel for critically reading the manuscript. This study was technically supported by use of the European Molecular Biology Laboratory EM core facility. Negative staining EM experiments were carried out in the laboratory of Hilmar Bading. We also thank the European Molecular Biology Laboratory Advanced Light Microscopy Facility team for their help with light microscopy and Leica for support of the facility. Reagents for expression of site-directed photolabile proteins in *E. coli* were generously provided by Dr. Peter G. Schultz. We thank Bernd Nürnberg for kindly providing antibodies directed against $G\alpha_s$.

This work was supported by grants from the Deutsche Forschungsgemeinschaft (SFB 638) to J.A.G. Briggs, B. Brügger, and F. Wieland.

Submitted: 8 November 2010
Accepted: 2 August 2011

References

Ambroggio, E., B. Sorre, P. Bassereau, B. Goud, J.B. Manneville, and B. Antonny. 2010. ArfGAP1 generates an Arf1 gradient on continuous lipid membranes displaying flat and curved regions. *EMBO J.* 29:292–303. doi:10.1038/emboj.2009.341

Antonny, B., I. Huber, S. Paris, M. Chabre, and D. Cassel. 1997. Activation of ADP-ribosylation factor 1 GTPase-activating protein by phosphatidylcholine-derived diacylglycerols. *J. Biol. Chem.* 272:30848–30851. doi:10.1074/jbc.272.49.30848

Austin, C., I. Hinners, and S.A. Tooze. 2000. Direct and GTP-dependent interaction of ADP-ribosylation factor 1 with clathrin adaptor protein AP-1 on immature secretory granules. *J. Biol. Chem.* 275:21862–21869. doi:10.1074/jbc.M908875199

Austin, C., M. Boehm, and S.A. Tooze. 2002. Site-specific cross-linking reveals a differential direct interaction of class 1, 2, and 3 ADP-ribosylation factors with adaptor protein complexes 1 and 3. *Biochemistry*. 41:4669–4677. doi:10.1021/bi016064j

Barlowe, C., L. Orci, T. Yeung, M. Hosobuchi, S. Hamamoto, N. Salama, M.F. Rexach, M. Ravazzola, M. Amherdt, and R. Schekman. 1994. COPII: a membrane coat formed by Sec proteins that drive vesicle budding from the endoplasmic reticulum. *Cell*. 77:895–907. doi:10.1016/0092-8674(94)90138-4

Beck, R., Z. Sun, F. Adolf, C. Rutz, J. Bassler, K. Wild, I. Sinning, E. Hurt, B. Brügger, J. Béthune, and F. Wieland. 2008. Membrane curvature induced by Arf1-GTP is essential for vesicle formation. *Proc. Natl. Acad. Sci. USA*. 105:11731–11736. doi:10.1073/pnas.0805182105

Beck, R., F. Adolf, C. Weimer, B. Bruegger, and F.T. Wieland. 2009a. ArfGAP1 activity and COPI vesicle biogenesis. *Traffic*. 10:307–315. doi:10.1111/j.1600-0854.2008.00865.x

Beck, R., M. Rawet, F.T. Wieland, and D. Cassel. 2009b. The COPI system: molecular mechanisms and function. *FEBS Lett.* 583:2701–2709. doi:10.1016/j.febslet.2009.07.032

Bigay, J., and B. Antonny. 2005. Real-time assays for the assembly-disassembly cycle of COP coats on liposomes of defined size. *Methods Enzymol.* 404:95–107. doi:10.1016/S0076-6879(05)04010-3

Bigay, J., P. Gounon, S. Robineau, and B. Antonny. 2003. Lipid packing sensed by ArfGAP1 couples COPI coat disassembly to membrane bilayer curvature. *Nature*. 426:563–566. doi:10.1038/nature02108

Boehm, M., R.C. Aguilar, and J.S. Bonifacino. 2001. Functional and physical interactions of the adaptor protein complex AP-4 with ADP-ribosylation factors (ARFs). *EMBO J.* 20:6265–6276. doi:10.1093/emboj/20.22.6265

Bremser, M., W. Nickel, M. Schweikert, M. Ravazzola, M. Amherdt, C.A. Hughes, T.H. Söllner, J.E. Rothman, and F.T. Wieland. 1999. Coupling of coat assembly and vesicle budding to packaging of putative cargo receptors. *Cell*. 96:495–506. doi:10.1016/S0092-8674(00)80654-6

Chardin, P., S. Paris, B. Antonny, S. Robineau, S. Béraud-Dufour, C.L. Jackson, and M. Chabre. 1996. A human exchange factor for ARF contains Sec7- and pleckstrin-homology domains. *Nature*. 384:481–484. doi:10.1038/384481a0

Dascher, C., and W.E. Balch. 1994. Dominant inhibitory mutants of ARF1 block endoplasmic reticulum to Golgi transport and trigger disassembly of the Golgi apparatus. *J. Biol. Chem.* 269:1437–1448.

Drin, G., and B. Antonny. 2005. Cell biology: helices sculpt membrane. *Nature*. 437:1247–1249. doi:10.1038/4371247a

Franco, M., P. Chardin, M. Chabre, and S. Paris. 1996. Myristoylation-facilitated binding of the G protein ARF1GDP to membrane phospholipids is required for its activation by a soluble nucleotide exchange factor. *J. Biol. Chem.* 271:1573–1578. doi:10.1074/jbc.271.3.1573

Helms, J.B., D. Helms-Brons, B. Brügger, I. Gkantiragas, H. Eberle, W. Nickel, B. Nürnberg, H.H. Gerdes, and F.T. Wieland. 1998. A putative heterotrimeric G protein inhibits the fusion of COPI-coated vesicles. Segregation of heterotrimeric G proteins from COPI-coated vesicles. *J. Biol. Chem.* 273:15203–15208. doi:10.1074/jbc.273.24.15203

Hsu, V.W., S.Y. Lee, and J.S. Yang. 2009. The evolving understanding of COPI vesicle formation. *Nat. Rev. Mol. Cell Biol.* 10:360–364. doi:10.1038/nrm2663

Krauss, M., J.Y. Jia, A. Roux, R. Beck, F.T. Wieland, P. De Camilli, and V. Haucke. 2008. Arf1-GTP-induced tubule formation suggests a function of Arf family proteins in curvature acquisition at sites of vesicle budding. *J. Biol. Chem.* 283:27717–27723. doi:10.1074/jbc.M804528200

Lee, M.C., L. Orci, S. Hamamoto, E. Futai, M. Ravazzola, and R. Schekman. 2005. Sar1p N-terminal helix initiates membrane curvature and completes the fission of a COPII vesicle. *Cell*. 122:605–617. doi:10.1016/j.cell.2005.07.025

Liu, Y., R.A. Kahn, and J.H. Prestegard. 2010. Dynamic structure of membrane-anchored Arf*GTP. *Nat. Struct. Mol. Biol.* 17:876–881. doi:10.1038/nsmb.1853

Long, K.R., Y. Yamamoto, A.L. Baker, S.C. Watkins, C.B. Coyne, J.F. Conway, and M. Aridor. 2010. Sar1 assembly regulates membrane constriction and ER export. *J. Cell Biol.* 190:115–128. doi:10.1083/jcb.201004132

Lundmark, R., G.J. Doherty, Y. Vallis, B.J. Peter, and H.T. McMahon. 2008. Arf family GTP loading is activated by, and generates, positive membrane curvature. *Biochem. J.* 414:189–194. doi:10.1042/BJ20081237

Malhotra, V., T. Serafini, L. Orci, J.C. Shepherd, and J.E. Rothman. 1989. Purification of a novel class of coated vesicles mediating biosynthetic protein transport through the Golgi stack. *Cell*. 58:329–336. doi:10.1016/0092-8674(89)90847-7

Malsam, J., A. Satoh, L. Pelletier, and G. Warren. 2005. Golgin tethers define subpopulations of COPI vesicles. *Science*. 307:1095–1098. doi:10.1126/science.1108061

Manneville, J.B., J.F. Casella, E. Ambroggio, P. Gounon, J. Bertherat, P. Bassereau, J. Cartaud, B. Antonny, and B. Goud. 2008. COPI coat assembly occurs on liquid-disordered domains and the associated membrane deformations are limited by membrane tension. *Proc. Natl. Acad. Sci. USA*. 105:16946–16951. doi:10.1073/pnas.0807102105

Matsuoka, K., L. Orci, M. Amherdt, S.Y. Bednarek, S. Hamamoto, R. Schekman, and T. Yeung. 1998. COPII-coated vesicle formation reconstituted with purified coat proteins and chemically defined liposomes. *Cell*. 93:263–275. doi:10.1016/S0092-8674(00)81577-9

McMahon, H.T., and J.L. Gallop. 2005. Membrane curvature and mechanisms of dynamic cell membrane remodelling. *Nature*. 438:590–596. doi:10.1038/nature04396

Nickel, W., and F.T. Wieland. 2001. Receptor-dependent formation of COPI-coated vesicles from chemically defined donor liposomes. *Methods Enzymol.* 329:388–404. doi:10.1016/S0076-6879(01)29100-9

Pucadyil, T.J., and S.L. Schmid. 2009. Conserved functions of membrane active GTPases in coated vesicle formation. *Science*. 325:1217–1220. doi:10.1126/science.1171004

Puertollano, R., P.A. Randazzo, J.F. Presley, L.M. Hartnell, and J.S. Bonifacino. 2001. The GGAs promote ARF-dependent recruitment of clathrin to the TGN. *Cell*. 105:93–102. doi:10.1016/S0092-8674(01)00299-9

Roux, A., K. Uyhazi, A. Frost, and P. De Camilli. 2006. GTP-dependent twisting of dynamin implicates constriction and tension in membrane fission. *Nature*. 441:528–531. doi:10.1038/nature04718

Rutz, C., A. Satoh, P. Ronchi, B. Brügger, G. Warren, and F.T. Wieland. 2009. Following the fate in vivo of COPI vesicles generated in vitro. *Traffic*. 10:994–1005. doi:10.1111/j.1600-0854.2009.00934.x

Serafini, T., and J.E. Rothman. 1992. Purification of Golgi cisternae-derived non-clathrin-coated vesicles. *Methods Enzymol.* 219:286–299. doi:10.1016/0076-6879(92)19029-6

Sönnichsen, B., R. Watson, H. Clausen, T. Misteli, and G. Warren. 1996. Sorting by COP I-coated vesicles under interphase and mitotic conditions. *J. Cell Biol.* 134:1411–1425. doi:10.1083/jcb.134.6.1411

Spang, A., K. Matsuoka, S. Hamamoto, R. Schekman, and L. Orci. 1998. Coatomer, Arf1p, and nucleotide are required to bud coat protein complex I-coated vesicles from large synthetic liposomes. *Proc. Natl. Acad. Sci. USA*. 95:11199–11204. doi:10.1073/pnas.95.19.11199

Stamnes, M.A., and J.E. Rothman. 1993. The binding of AP-1 clathrin adaptor particles to Golgi membranes requires ADP-ribosylation factor, a small GTP-binding protein. *Cell*. 73:999–1005. doi:10.1016/0092-8674(93)90277-W

Sun, Z., F. Anderl, K. Fröhlich, L. Zhao, S. Hanke, B. Brügger, F. Wieland, and J. Béthune. 2007. Multiple and stepwise interactions between coatomer and ADP-ribosylation factor-1 (Arf1)-GTP. *Traffic*. 8:582–593. doi:10.1111/j.1600-0854.2007.00554.x

Tabas, I., and S. Kornfeld. 1979. Purification and characterization of a rat liver Golgi alpha-mannosidase capable of processing asparagine-linked oligosaccharides. *J. Biol. Chem.* 254:11655–11663.

Tanigawa, G., L. Orci, M. Amherdt, M. Ravazzola, J.B. Helms, and J.E. Rothman. 1993. Hydrolysis of bound GTP by ARF protein triggers uncoating of Golgi-derived COP-coated vesicles. *J. Cell Biol.* 123:1365–1371. doi:10.1083/jcb.123.6.1365

Wang, L., A. Brock, B. Herberich, and P.G. Schultz. 2001. Expanding the genetic code of *Escherichia coli*. *Science*. 292:498–500. doi:10.1126/science.1060077

Weimer, C., R. Beck, P. Eckert, I. Reckmann, J. Moelleken, B. Brügger, and F. Wieland. 2008. Differential roles of ArfGAP1, ArfGAP2, and ArfGAP3 in COPI trafficking. *J. Cell Biol.* 183:725–735. doi:10.1083/jcb.200806140

Yang, J.S., S.Y. Lee, S. Spanò, H. Gad, L. Zhang, Z. Nie, M. Bonazzi, D. Corda, A. Luini, and V.W. Hsu. 2005. A role for BARS at the fission step of COPI vesicle formation from Golgi membrane. *EMBO J.* 24:4133–4143. doi:10.1038/sj.emboj.7600873

Zhao, L., J.B. Helms, B. Brügger, C. Harter, B. Martoglio, R. Graf, J. Brunner, and F.T. Wieland. 1997. Direct and GTP-dependent interaction of ADP ribosylation factor 1 with coatomer subunit beta. *Proc. Natl. Acad. Sci. USA*. 94:4418–4423. doi:10.1073/pnas.94.9.4418

Zhao, L., J.B. Helms, J. Brunner, and F.T. Wieland. 1999. GTP-dependent binding of ADP-ribosylation factor to coatomer in close proximity to the binding site for dilysine retrieval motifs and p23. *J. Biol. Chem.* 274:14198–14203. doi:10.1074/jbc.274.20.14198